Applied Physics A (2026) 132:228
https://doi.org/10.1007/s00339-026-09441-1

Applied Physics A
Materials Science & Processing

A comprehensive temperature-dependent impedance spectroscopy of dielectric behavior and AC conduction in Engineered Multi-Doped Oxide/Si Interfaces

Seda Bengi[1] · Seçkin Altındal Yerişkin[2] · Hayriye Gökçen Çetinkaya[3] · Ayşegül Dere[4] · Fahrettin Yakuphanoğlu[5]

Received: 13 October 2025 / Accepted: 16 February 2026
© The Author(s) 2026

Abstract

This study presents a comprehensive investigation of the dielectric-behavior, electric modulus response, AC conductivity, impedance, and phase angle of Al/(Zn: Cd: Ni: TiO_2)/p-Si MIS structures over the temperature range of 110–350 K and a bias interval of ±3 V, using impedance spectroscopy at 1 MHz. The real (ε′) and imaginary (ε″) parts of the dielectric constant were extracted from detailed capacitance and conductance measurements, demonstrating a clear dependence on both temperature and applied voltage. The increase in ε′ and ε″ with rising temperature and forward bias is attributed to enhanced interfacial-polarization, dipolar reorientation, space-charge effects, and thermally activated carriers. The electric modulus formalism, employed to analyze relaxation dynamics and suppress electrode polarization, revealed that the real part (M′) decreases with increasing temperature in both depletion and accumulation regions, while the imaginary part (M″) exhibits temperature-dependent peaks, indicative of dielectric relaxation and redistribution of interface states. The results suggest that short-range charge-transport and localized polarization dominate the dielectric response in different regimes of the applied field. Furthermore, the AC conductivity (σ_{AC}) increases with temperature, exhibiting an Arrhenius-type behavior. Two activation energies, approximately 5.6 meV at low temperatures and 18.9 meV at higher temperatures, were identified, implying the coexistence of distinct conduction mechanisms: shallow trap-assisted hopping at low temperatures and thermally activated carrier mobility at higher temperatures. These findings provide insights into the charge transport and polarization mechanisms governing the dielectric properties of Zn: Cd: Ni-doped TiO_2-based MIS structures.

Keywords Zn:Cd:Ni-doped TiO_2 · Temperature dependence · Dielectric behavior · Electric modulus · AC conductivity

1 Introduction

Metal–insulator–semiconductor (MIS) structures play a fundamental role in modern microelectronic and optoelectronic technologies, with widespread applications in sensors, transistors, and photovoltaic devices [1–5]. In such structures, the insulating interlayer situated between the metal and the semiconductor not only provides electrical isolation, but also directly influences charge transport, polarization behavior, and interface phenomena, thereby significantly determining the electrical characteristics and overall performance of the device. Therefore, a detailed investigation of the dielectric and electrical properties of the MIS interface is of great importance for improving both the reliability and functionality of these devices [6, 7]. The calculation of real and imaginary components of complex-dielectric (ε′, ε”), complex electric modulus (M’, M”), the

✉ Seda Bengi
sbengi@baskent.edu.tr

1 Vocational School of Technical Sciences, Başkent University, Ankara, Turkey

2 Vocational School of Technical Sciences, Gazi University, Ankara, Turkey

3 Vocational School of Health Services, Gazi University, Ankara, Turkey

4 Department of Electric and Energy, Vocational School of Technical Science, Firat University, Elazig, Turkey

5 Fytronix Electronic Technologies Company, Firat Teknokent, Elazig, Turkey

Published online: 25 February 2026

loss-tangent (tanδ), and the ac conductivity (σ_{ac}) of MIS type structures in wide range temperature and frequency would be beneficial to be informed on the polarization processes, relaxation process, conduction mechanism, the electronic-charges, and energy storage capacity of them. The polarization processes are usually called electronic, ionic, orientation and surface-charge polarizations and show high dependency on the frequency of the electric field as well as temperature. Therefore, Chemists, Physicists and Materials scientists are increasingly interested in studying the dielectric properties, relaxation processes, tanδ, and the σ_{ac} [5, 8]. AC conductivity, provides essential information on charge transport-mechanisms, trap-assisted hopping, and carrier mobility, which strongly influence leakage current, resistive switching behavior, frequency response, and temperature sensitivity.

In recent years, high-permittivity (high-k) dielectric materials have been proposed as alternatives to conventional SiO_2, offering several advantages such as increased capacitance density, reduced leakage current and lower power consumption [8–10]. Among them, titanium dioxide (TiO_2) has received considerable attention due to its wide band gap (~3.0–3.2 eV), excellent chemical stability, and high thermal resistance, making it an attractive candidate for integration into MIS structures [11–14]. Moreover, doping TiO_2 with metal ions such as Zn, Cd, and Ni has been shown to significantly alter its electrical conductivity, trap state density, energy band structure, and polarization mechanisms [15, 16]. These dopant-induced modifications are particularly promising for controlling temperature-dependent conduction and dielectric relaxation behavior.

Although TiO_2-based MIS devices have been extensively studied, research focusing on the combined effects of multi-metal doping and wide-range temperature variation on dielectric response, electric modulus, and ac conduction mechanisms remains relatively limited. In particular, the influence of interface trap-states on dielectric dispersion, conductivity, and relaxation dynamics continues to be a key subject of investigation. In this regard, electric modulus formalism has emerged as an effective analytical approach for evaluating relaxation processes, as it minimizes electrode polarization effects and helps distinguish between interfacial and bulk contributions [17].

The Al/(Zn: Cd: Ni: TiO_2)/p-Si structure explored in this study offers a promising platform for analyzing the impact of multi-element-doped TiO_2 interlayers on the temperature- and bias-dependent electrical behavior of MIS systems. Impedance spectroscopy measurements conducted over a broad temperature range (110–350 K) and applied voltage window (±3 V) were used to extract key parameters, including ε′, ε″, M′, M″, σAC, and phase angle (θ). Activation energies were calculated from Arrhenius plots to identify thermally activated conduction mechanisms, while electric modulus analysis provided deeper insight into the relaxation phenomena associated with interface states. The findings demonstrate the critical role of doped TiO_2 interfacial layers in interface engineering and highlight the potential of such structures for temperature-sensitive electronic device applications. Overall, the strong temperature and voltage dependence of the dielectric parameters, electric modulus spectra, and AC conductivity highlights the potential use of these MIS structures in advanced electronic devices, particularly for temperature-dependent capacitive sensors, dielectric modulators, and tunable high-k components. The integration of multi-element-doped TiO_2 via spin-coating technique further demonstrates the viability of this approach for developing functional and stable dielectric interfaces in semiconductor technology.

The main aim of this study is to systematically investigate a comprehensive temperature-dependent impedance spectroscopy of dielectric behavior and AC conduction in Engineered Multi-Doped Oxide/Si Interfaces. For this aim, the capacitance and conductance versus voltage (C-V, G/ω-V) measurement have been performed at enough high frequency (1 MHz) both over a wide temperature of 110 K-350 K and voltage range of ±3V to get more information on the ac conductivity (σ_{AC}), activation-energy (E_a), real and imaginary components of complex-dielectric (ε', ε"), and electric modulus (M', M") of the performed Al/(Zn: Cd: Ni: TiO_2)/p-Si MIS structures. All these parameters have been extracted from the measured C and G values for each temperature and voltage. The Arrhenius plot ($\ln(\sigma_{AC})$ vs q/kT) shows two linear regimes with different slopes which are corresponding to trap-assisted hopping at lower-temperatures and thermally activated conduction mechanism at higher-temperatures. The obtained higher value of ε' even at 1 MHz and room temperature indicated that the used multi-doped oxide/Si interfacial layer serves to significantly increase electronic charge or energy storage capacity of the MS structure.

2 Experimental details

Al/(ZnCdNi: TiO_2)/p-Si MIS type Schottky diodes (SDs) were fabricated using a (4:2:2:2) molar ratio of Zn, Cd, Ni, and TiO_2 as the interlayer. The devices were developed on boron-doped p-type silicon (p-Si) wafers with a (100) crystallographic orientation, a thickness of 300 μm, a diameter of 2 inches, and a resistivity in the range of 1–4 Ω·cm. Prior to the fabrication process, the p-Si substrates were ultrasonically cleaned using a standard cleaning protocol and subsequently dried under a stream of high-purity nitrogen (N_2) gas. Following the cleaning step, a 150 nm thick layer of

high-purity aluminum (99.999%) was thermally evaporated onto the entire backside of the Si wafer at a base pressure of 10^{-6} Torr. This layer was then annealed at 450 °C in a nitrogen atmosphere to form a low-resistivity Ohmic contact. For the preparation of the (ZnCdNi: TiO_2) interfacial layer, 0.3 M zinc acetate and 0.3 M cadmium acetate were each dissolved in 15 mL of solvent, while 0.3 M nickel chloride was dissolved in 20 mL of methoxymethane. These solutions were mixed separately for 30 min, after which a stabilizer was added, and the entire mixture was stirred for an additional 30 min. The final solution was combined according to the specified volume ratios and stirred for 2 h at room temperature, followed by aging for 48 h. The composite film was deposited onto the front surface of the p-Si substrate using a FYTRONIX 9000 static spin-coater which provides precise control over rotational speed, acceleration, and coating time. The system allows the implementation of static, dynamic, and multi-RPM spin-coating modes, enabling uniform and reproducible thin-film formation on semiconductor substrates. The deposition was performed in two layers at 1500 rpm for 30 s each. After the first coating, the sample was pre-heated at 150 °C for 15 min. Following the second layer deposition, the sample was heated at 150 °C for 30 min and then annealed at 450 °C for 1 h to improve crystalline and adhesion. The final film thickness was estimated to be approximately 100 nm. Subsequently, circular aluminum Schottky contacts with an area of 7.85×10^{-3} cm^2 and a thickness of 150 nm were thermally evaporated onto the interlayer at 10^{-6} Torr, completing the device structure. The electrical properties of the fabricated SDs were characterized using a HP-4192 A low-frequency impedance analyzer. Measurements were conducted in a temperature-controlled cryostat (VPF-475) over a temperature range of 110–350 K and applied voltage range of −3 V to +3 V at a fixed frequency of 1 MHz. The schematic structure, energy band diagram of the sample and measurement system are presented in Fig. 1(a), Fig. 1(b) and Fig. 1(c), respectively.

The C–V-T and G/ω–V-T measurements were performed using a computerized HP 4192 A LF impedance-analyzer in wide temperature range of 110–350 K and voltage range of ±3 V, respectively. Temperature control was done by using a lakeshore 321 auto-tuning temperature controller. Because the performed measurements covered only one/narrow temperature and voltage range they do not provide sufficient information on their electrical/dielectric characteristics, possible conduction and hopping mechanisms. But, when they are performed in the wide range temperature and voltage, they can provide more information to us both on electrical/dielectric characteristics, conduction, and hopping mechanisms. In addition, these measurements were carried out using a microprocessor and an IEEE-488 AC/DC converter card.

3 Results and discussion

It is well known that unless a special fabrication of MS with/without an interlayer, undesired many interface-traps can be formed at M/S interface with energy states in the bandgap (Eg) of semiconductor during the fabrication processes, disorders in the crystal structures, and chemical-composition of the interface. These traps act as recombination-centers and can capture or release many electrons under an external effect such as temperature, radiation, and electric-field. Therefore, today, the main scientific-problems are related to improving performance of these structures and decreasing their

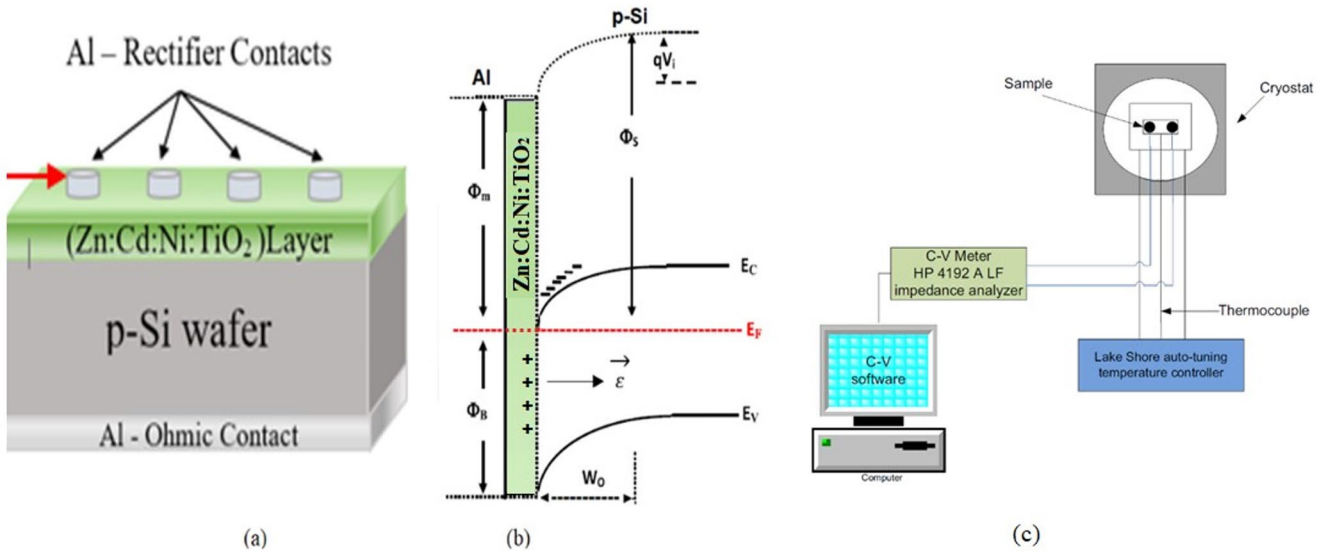


Fig. 1 (**a**) Schematic diagram, (**b**) energy-band diagram of the sample, and (**c**) measurement system

cost-production by developing some new materials as interfacial layer with high-dielectric (ε') [5, 6, 8, 9]. The conventional insulator-layer like SiO_2 at M/S interface by the traditional methods cannot passivate these active dangling-bonds at the semiconductor surface. The use of thin and high-dielectric interlayer (d_i) at M/S interface can increase the capacitance of MIS structure ($C=\varepsilon'(\varepsilon_o A/d_i)$), but there is a limitation to get thin interlayer and high surface area (A). High-dielectric interlayers are required to grow ultra-capacitors and other electronic charge/energy storage applications. Thus, doped-TiO_2 MIS structures s are mainly studied as high-k dielectric and interface-engineered structures rather than as direct logic transistors. Their principal applications include high-k dielectric research for advanced MIS/MOS technologies, memory devices (especially RRAM and charge-trapping memories), and sensing applications such as temperature, gas, and biosensors, due to their strong sensitivity to interface traps and temperature-dependent conductivity mechanisms.

The measurement of temperature dependent capacitance (C_m) and conductance (G_m) is a more important method for connecting the macroscopic measurements to the microscopic-charges movement in the electronic devices. Using the C_m and G_m values, the real and imaginary components of the dielectric constant (ε' and ε") can be calculated over the temperature range of 110–350 K and applied voltages up to ±3 V at a frequency range of 1 MHz [17–21]. The complex permittivity (ε^*) is given by:

$$\epsilon^* = \epsilon' - j\epsilon'' \tag{1}$$

Specifically, the real part of the dielectric constant (ε′) is determined from the following relation [17–21]:

$$\epsilon' = \frac{C_m.d_i}{A\epsilon_0} \tag{2}$$

Similarly, the imaginary part (ε″) is given by [17–21]:

$$\epsilon'' = \frac{G_m.d_i}{\omega A\epsilon_0} \tag{3}$$

where ω is the angular frequency, d_i is interlayer thickness. The loss tangent (tanδ) describes the fraction of energy lost as heat while the dielectric material is subjected to an external electric field. It is calculated as the ratio of ε″ to ε′, or equivalently [17–21]:

$$tan\delta = \frac{\epsilon''}{\epsilon'} = \frac{G_m}{\omega c_m} \tag{4}$$

These relations provide valuable insights into the dielectric behavior and energy dissipation characteristics of the material under investigation. The dielectric properties of the investigated material as a function of applied voltage (V) and temperature (T) are presented in Figs. 2–4. As shown in Fig. 2, the real part of the dielectric constant (ε') remains relatively low at low temperatures and voltages, while it exhibits a pronounced increase beyond approximately 1 V. Moreover, ε' systematically increases with rising temperature, indicating enhanced dipolar polarization and increased contribution from thermally activated charge carriers [22, 23]. The asymmetric rise in ε' at positive voltages suggests the presence of non-uniform polarization mechanisms within the material structure [5]. Figure 3 displays the imaginary part of the dielectric constant (ε"), which corresponds to dielectric losses. Like ε', ε" increases significantly with both voltage and temperature, particularly beyond 1 V and at higher temperatures. This behavior can

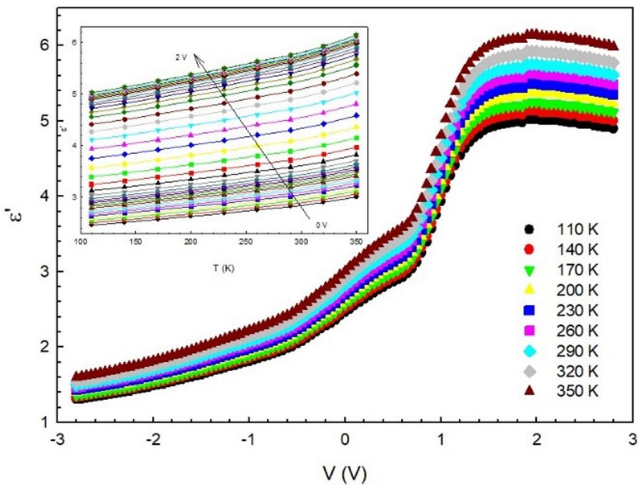


Fig. 2 Real dielectric (ε′) vs. voltage and temperature (110–350 K) at 1 MHz

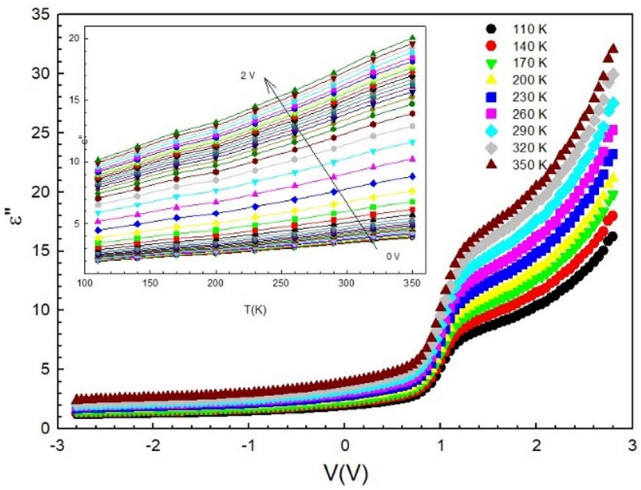


Fig. 3 Imaginary dielectric (ε″) vs. voltage and temperature (110–350 K) at 1 MHz

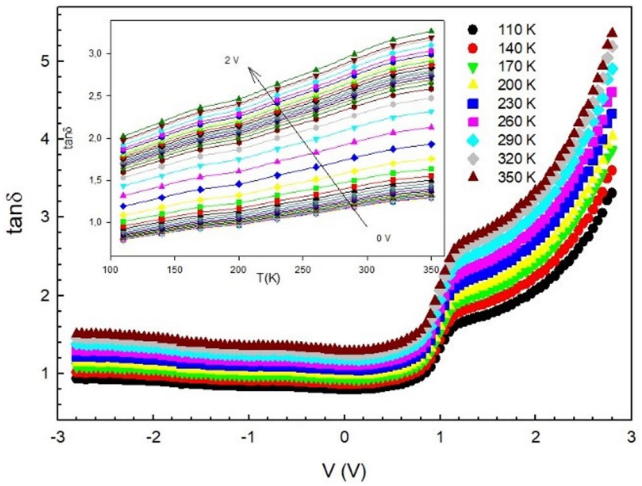


Fig. 4 Dielectric Loss Tangent (tan δ) vs. Voltage and Temperature (110–350 K) at 1 MHz

be attributed to increased ionic conductivity and enhanced mobility of charge carriers and defects [5, 9, 10, 12, 22–24]. As can be clearly seen from Figs. 2 and 3, while the value of ε' increases with increasing voltage until ay about 1.5V and then gives a broad peak for each temperature the value of ε" continues to increase in the whole measured bias voltage. Such behaviors of them are called as "inductive behavior" that is acts like a conductor due to the decrease of series resistance of sample. Figure 4 presents the loss tangent (tanδ = ε"/ε'), which also rises with increasing V and T, indicating that dielectric losses become more prominent under high-field and high-temperature conditions. Notably, all three parameters exhibit a marked change in behavior around 1–2 V, suggesting the activation of additional conduction or polarization mechanisms above a certain threshold voltage.

The insets in each figure illustrate the temperature dependence of ε', ε", and tanδ at 0 V and 2 V, revealing a clear and monotonic increase of these parameters with temperature. This trend is consistent with the enhanced thermal activation of carriers and the release of trapped charges at elevated temperatures [5, 9, 10, 12, 22–24]. Overall, the material exhibits strong temperature and voltage-dependent dielectric behavior, with higher polarization and losses observed under elevated conditions. These findings imply that careful control of operating temperature and voltage is crucial for optimizing the dielectric performance of the material, particularly in applications where low dielectric loss is required [5, 9, 10, 12, 22–24].

As seen in Figs. 2 and 3, especially in the strong accumulation region, the ε" value begins to increase rapidly while the ε' value begins to decrease. To see this behavior more clearly, the voltage-dependent variation of ε' and ε" values for 110, 230, and 350 K are given in Fig-5a, 5b, and 5c, respectively. As seen in Fig. 5, for each temperature, while the ε" value begins to increase in the accumulation region, ε' value begins to decrease. In other words, as the ε" value approaches its maximum, the ε' value begins to decrease. This behavior is known as inductive behavior in literature. That is, at sufficiently high positive bias voltages (accumulation region), it behaves like a conductor.

The presence of an interfacial layer at the metal/semiconductor (M/S) junction plays a crucial role in defining the electrical response of the structure by introducing additional capacitance effects. This interlayer imparts capacitive characteristics to the device, enabling the storage and modulation of electric charge, which is particularly important in high-frequency and sensor applications. In this context, the AC conductivity (σ_{AC}) of all fabricated structures was systematically derived from the dielectric loss component (ε")

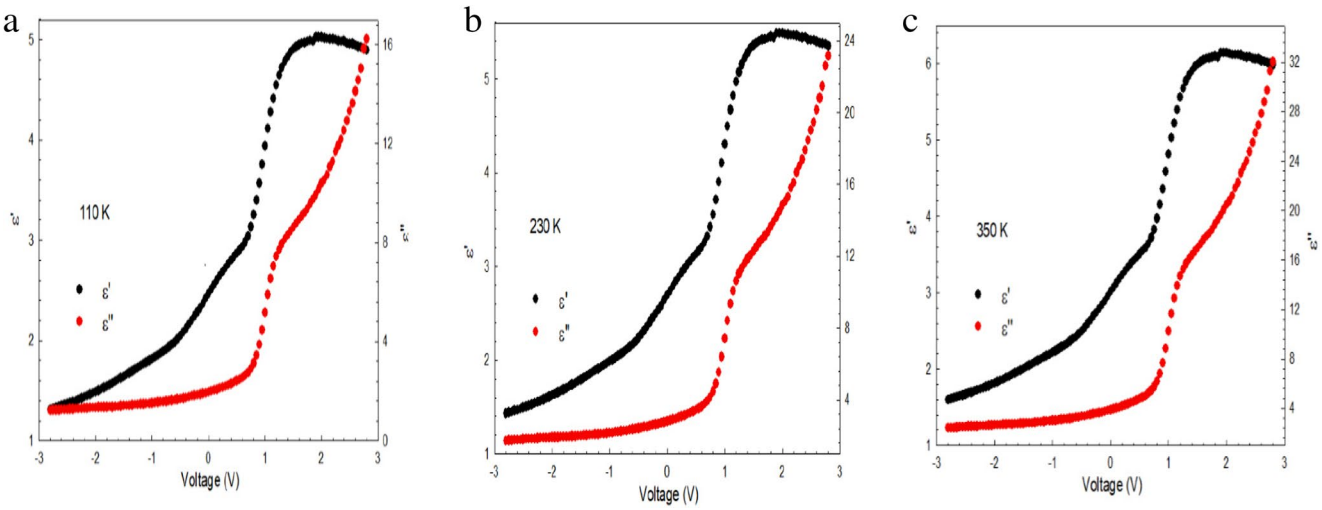


Fig. 5 The variation of ε and ε″ with voltage for the Al/(ZnCdNi: TiO_2)/p-Si MIS structure, (a) at 110 K, (b) at 230 K, and (c) at 350 K, respectively

of the complex permittivity, in accordance with the methodology outlined in previous studies [25–27]. This approach provides valuable insights into the charge transport and polarization mechanisms governing the overall dielectric behavior of the system.

$$\sigma_{ac} = \omega\, C tan\delta \left(d/a\right) = \epsilon'' \omega \epsilon_0 \quad (5)$$

Figure 6 demonstrates the variation of AC conductivity (σ_{AC}) as a function of applied bias voltage (V) for the Al/(Zn: Cd: Ni: TiO_2)/p-Si structure within the temperature range of 110 K to 350 K. The main graph reveals that σ_{AC} increases markedly with both temperature and applied voltage, particularly under forward bias conditions (V > 1.5 V). This enhancement is primarily attributed to the increased mobility of charge carriers and thermally activated hopping mechanisms that become prominent at elevated temperatures. Because the electrical conductivity ($\sigma = 1/\rho$) increases with increasing temperature due to the nature of semiconductors. In other words, electrical resistivity ($r = 1/\sigma$) decreases with increasing temperature due to the enhanced drift-mobility of electric-charge carriers, so allowing their easy move in the semiconductor. In the low-bias region (|V| < 1 V), σ_{AC} remains nearly invariant with respect to temperature, suggesting that the contribution of thermally excited carriers is minimal under weak electric fields. However, beyond a certain threshold voltage, σ_{AC} exhibits a pronounced increase, which is further amplified as temperature rises. This behavior indicates a thermally dependent charge transport mechanism, likely governed by thermally assisted tunneling and space charge limited conduction. The inset plot provides complementary insight into the temperature dependence of σ_{AC} at various fixed bias voltages between 0 V and 2 V. A consistent increase in conductivity with temperature is observed across all bias levels, reinforcing the thermally activated nature of the AC conduction process. The systematic upward trend with increasing temperature confirms that charge carrier dynamics in this MIS structure are significantly influenced by both thermal energy and the applied electric field.

Figure 7 presents the variation of the natural logarithm of AC conductivity ($\ln(\sigma_{AC})$) as a function of the inverse temperature (q/kT) for both low-temperatures (LTs) and high-temperatures (HTs) regimes. The linear behavior observed in both regions suggests a thermally activated conduction process, consistent with the Arrhenius-type relation [25]:

$$\sigma_{ac} = \sigma_0 exp\left(-qE_a/kT\right) \quad (6)$$

The activation energy (E_a) can be determined from the slope of the linear fits. As seen in Fig. 7, the plotted Arrhenius graph for 0.5 V has two linear regions with different slopes corresponding to high-temperature (HT) and low-temperature (LT) regions. For the high-temperature region, the activation energy (E_a) value is approximately 18.9 meV, while for the low-temperature region it is 5.6 meV. This indicates that two different conduction mechanisms are dominant at low and high temperatures. In other words, in the HTs region requires

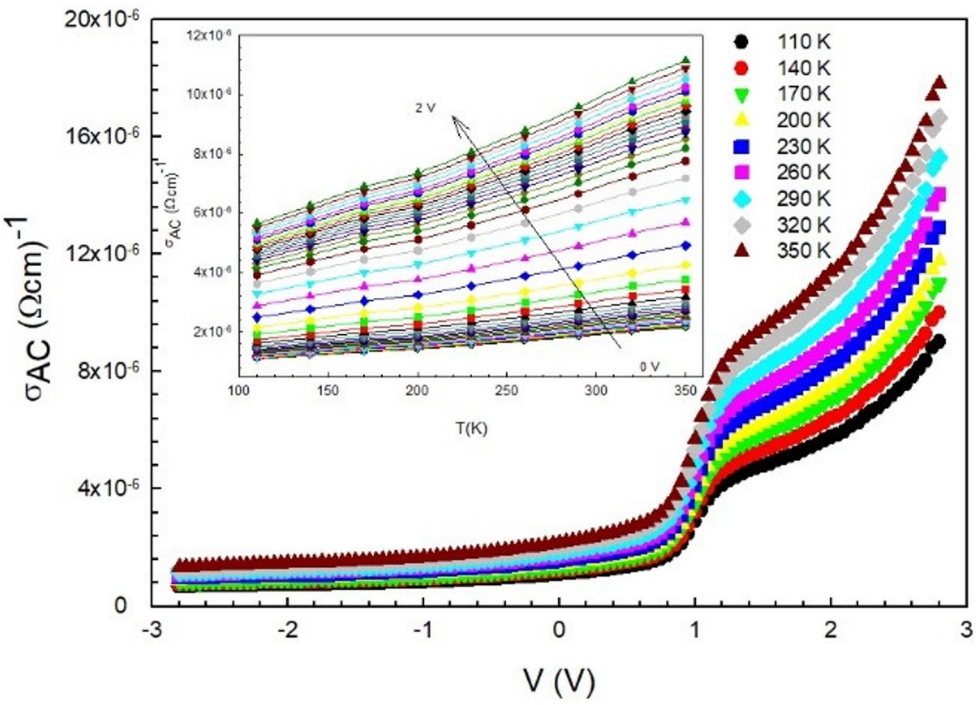


Fig. 6 AC conductivity (σ_{AC}) vs. voltage and temperature (110–350 K) at 1 MHz

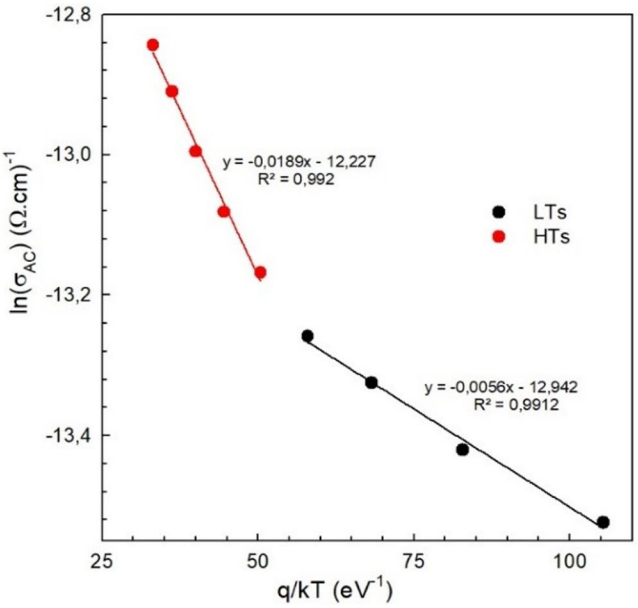


Fig. 7 Ln(σ_{AC}) vs. q/kT plot in temperature range of 110–350 K at 1 MHz

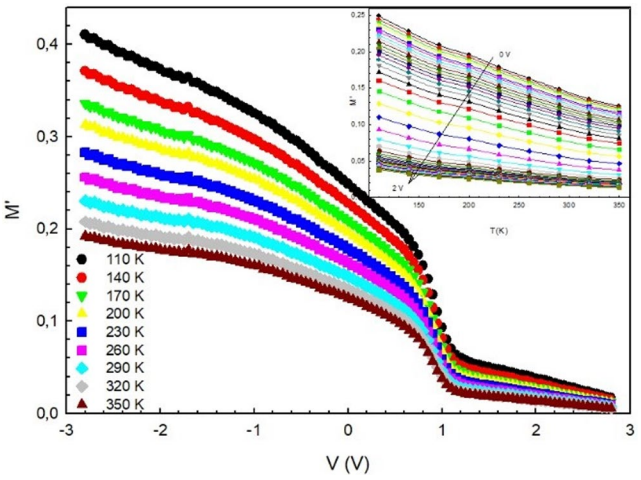


Fig. 8 Real part of electric modulus (M′) vs. voltage and temperature (110–350 K) at 1 MHz

higher thermal activation, likely due to increased phonon interactions or enhanced carrier hopping [25]. Conversely, the lower activation energy in the LTs region suggests that a different, less energy-dependent mechanism may dominate, possibly related to localized states or interface effects. The high linearity coefficients (R^2 = 0.992 for HTs and R^2 = 0.9912 for LTs) reinforce the reliability of the fits and confirm the temperature-dependent nature of AC conductivity in both regimes. This low value of E_a is associated with recombination, which causes even more departures from the thermionic-emission (TE) behavior at low and moderate temperatures [17, 21, 25]. According to these results, carriers are limited to localized movement, which suggests that there is less thermal activation at lower temperatures and that it begins to rise at higher temperatures because of thermal energy gained. The presence of dipole and interfacial polarizations (Maxwell-Wagner polarization) explains these phenomena.

The relaxation of the electric field in a thin interfacial layer at the M/S interface is generally explained by electric modulus. Another technique for illustrating the structure's dielectric response and exposing additional effects is complex modulus analysis. The dielectric characteristics of MPS structures are used to derive their complex electric modulus (M*) formalism. Therefore, the complex permeability (ε* = 1/M*) relationship is converted to the M* relationship using the formula below [17, 21, 26, 27].

$$M^* = 1/\epsilon^* = M' + jM'' = \epsilon'/\left(\epsilon'^2 + \epsilon''^2\right) + j\epsilon''/\left(\epsilon'^2 + \epsilon''^2\right) \quad (7)$$

where M' and M" are the real and the imaginary parts of complex modulus. Figure 8 presents the variation of the real part of the electric modulus (M′) as a function of applied voltage (V) for the Al/(Zn: Cd: Ni: TiO_2)/pSi structure at temperatures ranging from 110 K to 350 K. The M′ values exhibit a clear decrease with increasing voltage, particularly in the forward bias region, indicating a suppression of interfacial polarization effects at higher fields [5, 28–30]. Additionally, at a given voltage, M′ decreases with increasing temperature, which is typically associated with the increased mobility of thermally activated charge carriers and the subsequent reduction in bulk resistance. The inset graph further demonstrates the temperature dependence of M′ at selected bias voltages between 0 V and 2 V. The systematic decrease of M′ with temperature supports the idea that the relaxation phenomena within the structure is temperature-dependent and influenced by the redistribution of space charge. The observed behavior suggests that at elevated temperatures, charge carriers become more delocalized, leading to a reduction in the electric field buildup across the interfacial regions [5, 28–30].

Figure 9 illustrates the variation of the imaginary part of the electric modulus (M″) with applied voltage for the same MIS structure over the same temperature range. Like M′, the M″ values also show a general decreasing trend with increasing voltage [5, 28–30]. The pronounced peaks typically seen in M″–V or M″–f plots, which correspond to relaxation processes, appear suppressed or shifted at higher temperatures, indicating a strong temperature dependence of dielectric relaxation mechanisms [5, 28–30]. The inset of Fig. 9 shows the variation of M″ with temperature at different fixed voltages (from 0 V to 2 V). A consistent decrease in M″ with increasing temperature is evident, reflecting the thermally activated relaxation of dipoles and the diminished influence of space charge polarization. This behavior is in line with the Maxwell–Wagner relaxation model, where the reduction in M″ at higher temperatures implies

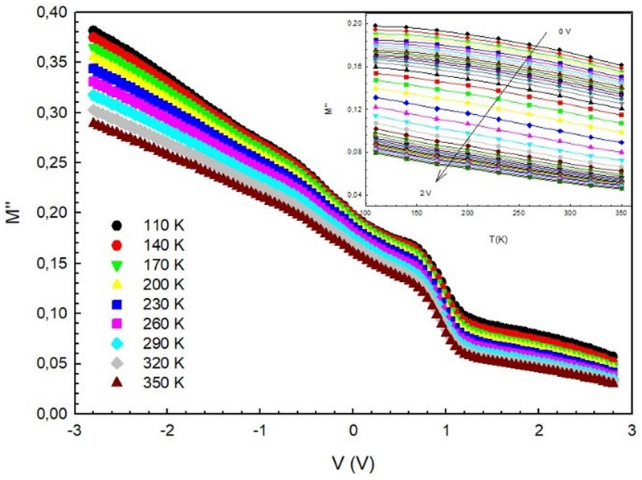


Fig. 9 Imaginary part of electric modulus (M″) vs. voltage and temperature (110–350 K) at 1 MHz

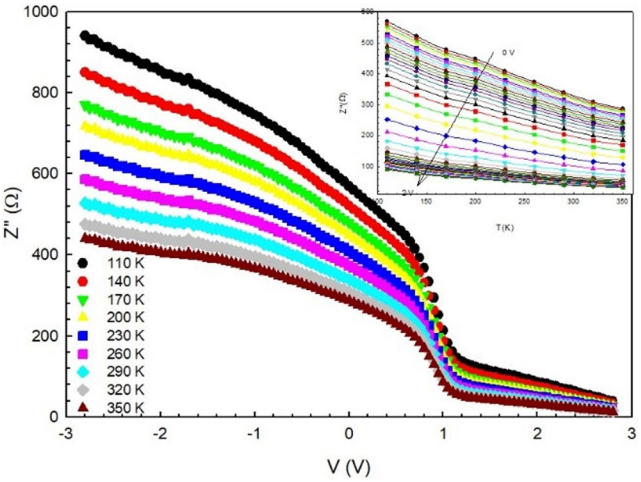


Fig. 11 Imaginary part of impedance (Z″) vs. Voltage and Temperature (110–350 K) at 1 MHz

a faster relaxation process due to increased carrier mobility and reduced impedance at grain boundaries or interfacial regions [5, 28–30].

One method for examining the dielectric characteristics of interfacial materials is complex impedance spectroscopy (IS). Thus, a complex impedance (Z*) can be used to investigate the materials' dielectric behavior. The Z^* and its real (Z') and imaginary components (Z'') can be extracted with the following relations [31–34];

$$Z^* = \frac{1}{i\omega C_o \epsilon^*} = Z' - jZ'' = \frac{\epsilon''}{\omega C_o (\epsilon'^2 + \epsilon''^2)} - j\frac{\epsilon'}{\omega C_o (\epsilon'^2 + \epsilon''^2)} \quad (8)$$

Figures 10 and 11 present the variations of the real (Z′) and imaginary (Z″) components of the complex impedance as functions of applied voltage and temperature, measured at a fixed frequency of 1 MHz in the temperature range of 110–350 K. The results show that Z′ exhibits a distinct peak in the voltage range of approximately 1–1.5 V at all investigated temperatures. This peak is commonly attributed to the presence of interfacial charges and surface states (Nss) at the metal–semiconductor interface, which can trap and emit carriers depending on the biasing conditions. Conversely, Z″ demonstrates a sharp decline in the same voltage region where Z′ reaches its maximum. This complementary behavior between Z′ and Z″ reflects a transition in the charge transport mechanism, where the release of trapped charges at the interface reduces the energy loss (represented by Z″) and enhances the capacitive response (reflected in Z′). Such temperature dependence suggests that higher temperatures facilitate carrier mobility and the depopulation of interfacial traps, thereby modulating the impedance characteristics.

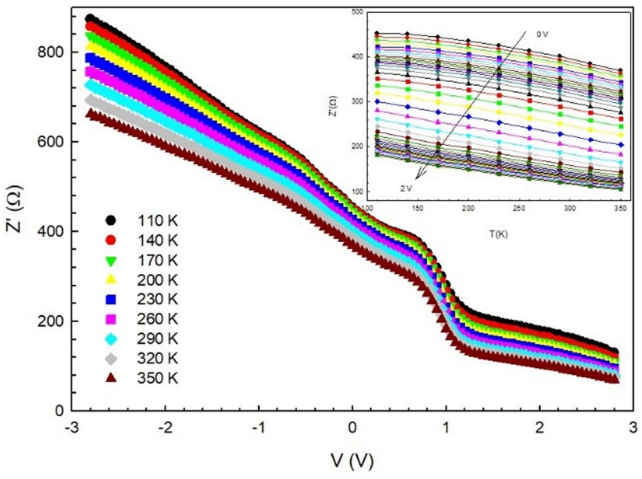


Fig. 10 Real part of impedance (Z′) vs. Voltage and Temperature (110–350 K) at 1 MHz

Based on impedance measurements, the following expression is used to calculate the phase angle (θ°) between resistive and capacitive currents [31–33];

$$\theta = tan^{-1}\left(\frac{Z''}{Z'}\right) \quad (9)$$

Figure 12 illustrates the phase angle (θ) as a function of applied voltage at various temperatures. As the bias approaches 0 V, θ undergoes a rapid decline, reaching a minimum at forward-bias voltages. This sharp reduction in phase angle reflects the increasing influence of resistive (conductive) components of the impedance, signifying a shift from dielectric to conductive behavior of the structure. The temperature dependence of θ suggests that the onset of conduction at forward bias is thermally activated, as expected for charge injection and transport processes in such interfacial systems.

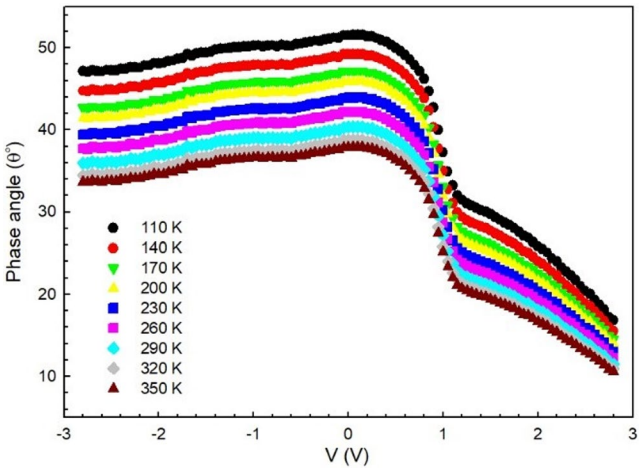


Fig. 12 Variation of phase angle (θ) with applied voltage at different temperatures (110–350 K)

In light of the above explanations, we can say that the main important issue is related to increasing the performance of MIS type structures and decreasing the cost-production by developing some new materials as an interlayer with high-dielectric (ε') [32–39]. While conventional low-ε' SiO_2 films are both stable and readily available, they cannot reduce leakage currents, interface traps in these devices to the desired level. Instead, some metal oxides and polymers that are easy to grow can be used, but they have both low conductivity and dielectric constants. The most important and easiest way to increase these is to dope them with materials such as metal or graphene in appropriate proportions. Thus, the prepared high-dielectric interlayer (d_i) at M/S interface leads to an important increase in the value of capacitance and storage electrons or energy storage capacity ($C_i=\varepsilon'\varepsilon_o A/d_i$)) and regulate conduction mechanisms and passivated many interface traps. Thus, the use of high-dielectric interlayer at M/S interface makes these devices more sensitive to temperature, light, and radiation, so making them suitable for use in optical/thermal sensor and charge-trapping applications.

The successful implementation of the spin-coated Zn: Cd: Ni-doped TiO_2 interlayer validates this fabrication method as an effective and scalable approach for engineering stable, reproducible, and high-performance dielectric interfaces. Furthermore, the successful integration of the TiO_2 interlayer doped with Zn, Cd, and Ni elements via the spin coating technique substantiates this method as an effective and feasible approach for producing stable, reproducible, and functional dielectric interfaces in semiconductor technology. The findings highlight the advantages provided by multi-element doping in interface engineering and pave the way for the development of high-performance, temperature-controlled electronic devices in the future. Similar results have been also reported by various scientists on the temperature, frequency, and voltage dependence of dielectric properties, AC conductivity, electric modulus, and phase angle in MIS type structures [35–38].

4 Conclusions

This study has provided a detailed and systematic analysis of the dielectric, impedance, electric modulus, and AC conductivity characteristics of Al/(Zn: Cd: Ni: TiO_2)/p-Si MIS structures as a function of temperature and applied voltage. The results reveal a strong and intricate dependence of the dielectric parameters (ε′, ε″, and tan δ) on both external stimuli, reflecting the interplay between interfacial polarization, dipolar reorientation, space-charge effects, and thermally activated charge carriers. The significant enhancements observed in ε′ and ε″ with increasing temperature and forward bias underscore the prominent role of interface states and localized dipole dynamics, which dominate the polarization processes in these structures. Likewise, the steady increase of tanδ at elevated conditions highlights the growing energy dissipation due to intensified charge dynamics and redistribution of trapped carriers. The electric modulus formalism provided valuable insights into the relaxation mechanisms of the system. The observed decrease in M′ with increasing temperature and forward bias suggests a reduction in bulk resistance and an enhancement in carrier mobility. Additionally, the temperature-dependent peaks in M″ indicate the dynamic redistribution and depopulation of interface traps, reflecting a transition toward faster relaxation regimes at elevated temperatures. AC conductivity measurements further substantiated these findings by revealing a clear transition between conduction mechanisms: shallow trap-assisted hopping dominating at low temperatures and thermally activated carrier transport prevailing at elevated temperatures, as evidenced by the two distinct activation energies derived from Arrhenius analysis. Impedance spectroscopy and phase angle measurements complemented the dielectric and modulus analyses, demonstrating a pronounced peak in Z′ and a steep decline in Z″ at forward biases around 1–1.5 V, corresponding to the release of trapped carriers and an enhanced capacitive response. The observed reduction in phase angle from its near-ideal capacitive value at reverse bias toward a more resistive behavior under forward bias reflects the increasing contribution of free carriers and conductive pathways as the applied field strengthens. As a result, these findings provide a comprehensive picture of the underlying charge transport and polarization phenomena in Zn: Cd: Ni-doped TiO_2-based MIS structures. The strong sensitivity of all measured parameters to temperature and bias conditions not only emphasizes the dominant role of interfacial phenomena and thermally activated dynamics but also confirms the capability of such multi-doped dielectric layers to tune and enhance the functional properties of MIS devices.

Acknowledgements This work has been supported by TUBITAK with the research-project number-121C458 and Gazi University Scientific Research Project (BAP) with FYL-2024-9859.

Author Contributions S. Bengi: Writing-review & editing, Writing-original draft, Visualization, Validation, Supervision, S.A. Yerişkin: Writing-review & editing, H.G. Çetinkaya Writing-review & editing, A. Dere: Methodology, F. Yakuphanoglu: Methodology.

Funding Open access funding provided by the Scientific and Technological Research Council of Türkiye (TÜBİTAK).

Data availability The data cannot be made publicly available upon publication because no suitable repository exists for hosting data in this field of study. The data that support the findings of this study are available on reasonable requests from the authors.

Declarations

Ethical approval This study does not contain any human-related information, and no animals were used.

Conflict of interest the author has not disclosed any competing interests.

Open Access This article is licensed under a Creative Commons Attribution 4.0 International License, which permits use, sharing, adaptation, distribution and reproduction in any medium or format, as long as you give appropriate credit to the original author(s) and the source, provide a link to the Creative Commons licence, and indicate if changes were made. The images or other third party material in this article are included in the article's Creative Commons licence, unless indicated otherwise in a credit line to the material. If material is not included in the article's Creative Commons licence and your intended use is not permitted by statutory regulation or exceeds the permitted use, you will need to obtain permission directly from the copyright holder. To view a copy of this licence, visit http://creativecommons.org/licenses/by/4.0/.

References

1. S.M. Sze, K.K. Ng, *Physics of Semiconductor Devices* (Wiley, Hoboken), 2006)
2. B.L. Sharma, *Metal-Semiconductor Schottky Barrier Junctions and Their Applications* (Plenum, New York, 1984)
3. E.H. Rhoderick, R.H. Williams, *Metal Semiconductor Contacts* (Clarendon, Oxford, 1988)
4. J. Kim, G. Hwi An, S. Bang, D. Geun Park, D. Kim, S. Jin, M. Jung Kim, H. Seok Lee, J. Woo, Lee, Comparative analysis of Schottky barriers for heterogeneous defect domains in monolayer WS2 field-effect transistors. Appl. Surf. Sci. **604**, 154600 (2022)
5. A. Tataroğlu, H. Durmuş, A.F. Vahid, B. Avar, Ş. Altındal, High-temperature sensitivity complex dielectric/electric modulus, loss tangent, and AC conductivity in Au/(S:DLC)/p-Si (MIS) structures. J. Mater. Sci.: Mater. Electron. **35**, 227 (2024)
6. Ş, A.F. Altındal, Ş. Özdemir, A. Aydoğan, Türüt, Discrepancies in barrier heights obtained from current–voltage (IV) and capacitance–voltage (CV) of Au/PNoMPhPPy/n-GaAs structures in wide range of temperature. J. Mater. Sci. Mater. Electron. **33**, 12210–12223 (2022)
7. T. Çakıcı, A. Ajjaq, A.O. Çağırtekin, Ö. Barin, M. Özdal, S. Acar, Surface activation of Si-based Schottky diodes by bacterial biosynthesized AgInSe2 trimetallic alloy nanoparticles with evidenced negative capacitance and enhanced electro-dielectric performance. Appl. Surf. Sci. **631**, 157522 (2023)
8. Q.X. Zhang, The Electrical Performances and Leakage Current Conduction Mechanism of $Al_2O_3/ZrO_2/SiO_2/ZrO_2/Al_2O_3$ MIM Capacitors. Integr. Ferroelectr. **217**, 233–239 (2021)
9. T. Akila, V. Balasubramani, D.S. Priya, G. Alan Sibu, K.A. Alibrahim, M. Muthuramamoorthy, Investigation of Pr7O12 thin-film-based Cu/Pr7O12/n-Si MIS Schottky barrier diodes for enhanced photosensitivity. J. Mater. Sci: Mater. Electron. **36**, 2150 (2025)
10. A. Seçkin, H. Koralay, Electrical Properties of Schottky Devices from HfO2 and ZnO/HfO2 Thin Films: Morphological, Structural, and Optical Investigations. ACS Omega. **10**, 6520–6533 (2025)
11. Y.A. Kalandaragh, H.I. Efkere, A. Barkhordari, B. Marmiroli, B. Sartori, S. Özçelik, G.R. Pirgholi-Givi, Ş. Altındal, Effect of TiO_2-Surfactant Interface on the Electrical and Dielectric Properties of a Metal–Insulator–Semiconductor (MIS) Structure, J. Electron. Mater. **54,** 2388–2403 (2025)
12. R. Li, M. Sun, Y. Ma, S. Li, L. Wang, Y. Cui, Improved visible-light-dielectric response in self-doped rutile TiO2. J. Alloys Compd. **1010**, 177134 (2025)
13. F. Unal, M.S. Kurt, S. Durdu, Investigation of the effect of light on the electrical parameters of Si/TiO2 heterojunctions produced by anodic oxidation on p-type Si wafer. J. Mater. Sci: Mater. Electron. **33**, 15834–15847 (2022)
14. E. Dikicioğlu, M.B. Balı, S. Sağlam, H. Berberoğlu, I. Pavlov, A. Goodarzi, E. Orhan, Electrical Properties of Laser Patterned Schottky Diode with ALD-Grown TiO2 Interlayer. ACS Omega. **9**, 21346–21352 (2024)
15. H. Kim, The Temperature-Dependent Interface States and the Reverse Current Conduction Mechanism of Single-Crystal ZnO Schottky Diodes. Mater. Trans. **66**, 153–159 (2025)
16. T.A. Abdel-Baset, A.H. Bashal, Structure and AC conductivity of zinc and nickel-doped TiO2 nanocomposite synthesized by simple incipient wet impregnation method. J. Mater. Sci: Mater. Electron. **31**, 18533–18540 (2020)
17. A. Chelkowski, *Dielectric Physics* (Elsevier, Amsterdam), 1980)
18. C.P. Symth, *Dielectric Behaviour and Device* (McGraw-Hill, New York, 1955)
19. A.R. von Hippel, *Dielectric Materials and Applications* (John Willey &Sons. Inc., New York, 1954)
20. V.V. Daniel, *Dielectric Relaxation* (Academic, London) (1967)
21. M. Popescu, I. Bunget, *Physics of Solid Dielectrics* (Elsevier, Amsterdam), 1984)
22. Ç.Ş. Güçlü, Ş. Altındal, M. Ulusoy, The study of the dependence of dielectric properties, electric modulus, and AC conductivity on the frequency and voltage in the Au/(CdTe:PVA)/nSi (MPS) structures. J. Mater. Sci.: Mater. Electron. **35**, 1225 (2024)
23. Y. Şafak, A.F. Vahid, N. Başman, H.G. Çetinkaya, Ş. Altındal, Frequency-dependent electrical parameters and extracted voltage-dependent surface states in Al/DLC/p-Si structure using the conductance method. Appl. Phys. A **129**, 358 (2023)
24. H.G. Çetinkaya, O. Çiçek, Ş. Altındal, Y. Badali, S. Demirezen, Vertical CdTe:PVP/p-Si - Based Temperature Sensor by Using Aluminum Anode Schottky Contact. IEEE Sens. J. **22**, 22391–22397 (2022)
25. R.B. Bozkurt, E. Evcin Baydilli, A. Kaymaz, Ş. Altındal, H. Durmuş, Dielectric properties and polarization mechanisms of the DLC-interlayered Schottky structures under low-moderate and high-temperatures. Mater. Sci. Engineering: B **320**, 118406 (2025)
26. Ö. Sevgili, İ. Taşçıoğlu, S. Boughdachid, Y. Azizian-Kalandaraghd, Ş. Altındal, Examination of dielectric response of Au/HgS-PVA/n-Si (MPS) structure by impedance spectroscopy method. Phys. B: Condens. Matter. **566**, 125 (2019)

27. Ş. Altındal, A. Barkhordari, Y. Azizian-Kalandaragh, B.S. Çevrimli, H.R. Mashayekhi, Dielectric properties and negative-capacitance/dielectric in Au/n-Si structures with PVC and (PVC: Sm2O3) interlayer. Mater. Sci. Semiconduct. Process. **147**, 106754 (2022)
28. F. Ahmad, A. Maqsood, Complex impedance, dielectric constant, electric modulus, and conductivity analysis of Cd doped ZnO nanostructures at high temperatures. Phys. E. **143**, 115353 (2022)
29. E.G. El-Metwally, N.A. Hegab, M. Mostfa, The ac conduction mechanism and dielectric relaxation behavior of amorphous Te81Ge15Bi4 chalcogenide glass thin films. J. Mater. Sci. **33**, 12384–12396 (2022)
30. B. Gowtham, V. Balasubramani, S. Ramanathan, M. Ubaidullah, S.F. Shaikh, G. Sreedevi, Dielectric relaxation, electrical conductivity measurements, electric modulus and impedance analysis of WO3 nanostructures. J. Alloys Compd. **888**, 161490 (2021)
31. S. Demirezen, S.A. Yerişkin, Frequency and voltage-dependent dielectric spectroscopy characterization of Al/(Coumarin-PVA)/p-Si structures. J. Mater. Sci. Mater. Electron. **32**, 25339 (2021)
32. A.M. Akbaş, A. Tataroğlu, Ş. Altındal, Y. Azizian-Kalandaragh, Frequency dependence of the dielectric properties of Au/(NG:PVP)/n-Si structures. J. Mater. Sci. Mater. Electron. **32**, 7657 (2021)
33. Y.Ş. Asar, Ö. Sevgili, Ş. Altındal, Investigation of dielectric relaxation and AC conductivity in Au/(carbon nanosheet-PVP composite)/n-Si capacitors using impedance measurements. J. Mater. Sci.: Mater. Electron. **34**, 893 (2023)
34. M.T. Güneşer, H. Elamen, Y. Badali, Ş. Altíndal, Frequency dependent electrical and dielectric properties of the Au/(RuO2: PVC)/n-Si (MPS) structures. Phys. B: Condens. Matter. **657**, 414791 (2023)
35. N. Hamdaoui, Y. Azizian-Kalandaragh, M. Khlifie, L. Beji, Structural, magnetic and dielectric properties of $Ni_{0.6}Mg_{0.4}Fe_2O_4$ ferromagnetic ferrite prepared by sol gel method. Ceram. Int. **45**, 16458–16465 (2019)
36. C.B. Makhlouf, M.L. Bouazizi, S. Hcini, H.B. Bacha, L. HajTaieb, M. Gassoumi, Detailed structural study, optical, and dielectric properties of Co0.4Ni0.3Zn0.3Fe2O4 ferrite and its potential applications for optoelectronic and electronic devices. J. Solgel Sci. Technol. **16**, 378–401 (2025)
37. R.B. Bozkurt, E.E. Baydilli, A. Kaymaz, Ş. Altındal, H. Durmus, Dielectric properties and polarization mechanisms of the DLC-interlayered Schottky structures under low-moderate and high-temperatures. Mater. Sci. Eng., B **320**, 118406 (2025)
38. A. Kaya, S. Alialy, S. Demirezen, M. Balbaşı, S.A. Yerişkin, A. Aytimur, The investigation of dielectric properties and AC conductivity of Au/GO-doped PrBaCoO nanoceramic/n-Si capacitors using impedance spectroscopy method. Ceram. Int. **42**, 3322–3329 (2016)
39. A. Khalkhali, E. Erbilen Tanrıkulu, S. Altındal Yerişkin, A. Arslan, K. Alsaç, Yıldız, A Study Regarding Dielectric Response and ac Electrical Conductivity of Schottky Structures (SSs) Interlaid with (Fe_3O_4-PVA) by Using Dielectric Spectroscopy Method. J. Inorg. Organomet. Polym. **35**, 6440–6457 (2025)

Publisher's note Springer Nature remains neutral with regard to jurisdictional claims in published maps and institutional affiliations.